



Thin film structural color is widespread in slime molds (Myxomycetes, Amoebozoa)

VIOLA BAUERNFEIND,^{1,2}  ANNA RONIKIER,³ 
MICHAŁ RONIKIER,³  GREGOR KOZŁOWSKI,⁴ 
ULLRICH STEINER,^{1,2}  AND BODO D. WILTS^{2,5,*} 

¹Adolphe Merkle Institute, University of Fribourg, Fribourg, Switzerland

²Swiss National Center for Competence in Research (NCCR) Bio-inspired Materials, University of Fribourg, Fribourg, Switzerland

³W. Szafer Institute of Botany, Polish Academy of Sciences, Kraków, Poland

⁴Department of Biology and Botanical Garden, University of Fribourg, Fribourg, Switzerland

⁵Department of Chemistry and Physics of Materials, University of Salzburg, Salzburg, Austria

*bodo.wilts@plus.ac.at

Abstract: Brilliant colors in nature arise from the interference of light with periodic nanostructures resulting in structural color. While such biological photonic structures have long attracted interest in insects and plants, they are little known in other groups of organisms. Unexpected in the kingdom of Amoebozoa, which assembles unicellular organisms, structural colors were observed in myxomycetes, an evolutionary group of amoebae forming macroscopic, fungal-like structures. Previous work related the sparkling appearance of *Diachea leucopodia* to thin film interference. Using optical and ultrastructural characterization, we here investigated the occurrence of structural color across 22 species representing two major evolutionary clades of myxomycetes including 14 genera. All investigated species showed thin film interference at the peridium, producing colors with hues distributed throughout the visible range that were altered by pigmentary absorption. A white reflective layer of densely packed calcium-rich shells is observed in a compound peridium in *Metatrichia vesparium*, whose formation and function are still unknown. These results raise interesting questions on the biological relevance of thin film structural colors in myxomycetes, suggesting they may be a by-product of their reproductive cycle.

© 2024 Optica Publishing Group under the terms of the [Optica Open Access Publishing Agreement](#)

1. Introduction

Structural color results from the interference of light with periodic structures that have a periodicity on the length scale of the wavelength of visible light. Varying interference conditions usually make structural color iridescent, i.e., the perceived color depends on the observation and viewing angle [1]. Disorder in photonic structures can result in angle-independent colors [2–4] and for random structures lead to broad-band scattering, producing white without absorption [5–8]. The presence of pigments in disordered structures, in contrast, always results in angle-independent colors due to wavelength-selective absorption of light [9–11]. Pigments can further alter the optical response of photonic nanostructures and limit iridescence [10–13].

The majority of plant colors arise from pigments, but some species developed photonic nanostructures in the form of thin films, multilayers, diffraction gratings, and other, more complex, surface morphologies [1,14–20]. The comparably well-investigated plants are outnumbered by other, poorly studied biological groups, such as speciose fungi with an estimated 2.2 – 3.8 million species [21,22]. While to this day not reported in true fungi (Eumycetes) [23], slime molds (Myxomycetes) that were previously classified as fungi [24], have been shown to feature structural color. This group is currently classified in the kingdom Amoebozoa [25], which contains unicellular organisms. In their life cycle, myxomycetes form active single-cell

myxamoebae and multinuclear plasmodia as well as static fruiting bodies. The fruiting bodies are complex, macroscopic structures (typically up to 5 mm in diameter), which bear haploid spores and comprise several plasmodium-derived structures such as columella, capillitium, and peridium. The peridium is a single or multilayered wall surrounding the spore-filled structure (sporothece). In *Diachea leucopodia*, the only myxomycete studied so far optically, the pointillistic appearance of sporothecae results from thin film interference at the approximately 300 nm to 700 nm thick peridium [26–28]. Thin film interference is well understood and widespread [1], e.g. in insect wings [29–32], and plants [33,34], but has not been investigated systematically in myxomycetes. In contrast, pigmentary coloration in myxomycetes is well-studied with many reported chemical compounds [35–39]. While the structural peridium colors in myxomycetes have not been shown to serve a biological purpose, they are nevertheless an important trait for characterizing myxomycete species as they contribute to the optical appearance of the fruit bodies. The presence of iridescence and its coloration are morphological characters used to identify species and species groups in some genera, especially in the genus *Lamproderma* [28,40].

To gain in-depth insight into the presence and origin of structural colors in myxomycetes, we investigated a comprehensive set of 22 species (Supplement 1, Table S1). These represented the two major evolutionary clades of myxomycetes [41,42], the so-called bright-spored group (the genera *Arcyria*, *Calomyxa*, *Cribraria*, *Dianema*, *Licea* and *Metatrachia*) and the dark-spored group (the genera *Badhamia*, *Comatracha*, *Diachea*, *Diderma*, *Didymium*, *Lamproderma* and *Meriderma*) and were studied using light microscopy, optical spectroscopy and ultrastructural characterization. Two specimens were further investigated for their material composition and scattering behavior using energy-dispersive X-ray spectroscopy (EDXS) and finite-difference time-domain (FDTD) modeling.

2. Results

2.1. Light microscopy reveals colorful peridia in all studied myxomycetes species

If large enough to be seen with the bare eye, the studied sporothecae with diameters between about 100 μm and 5 mm appear in dark hues of green, blue, brown, or purple.

To characterize the optical properties of the sporothecae, we recorded bright- and dark-field reflectance micrographs at different magnifications, which are summarized in Supplement 1, Table S2 (Columns 1-4) in the Supplement 1. Bright-field reflectance micrographs of four selected species, *Lamproderma cristatum*, *Cribraria argillacea*, *Diderma meyeriae* and *Metatrachia vesparium*, are shown in Fig. 1(a-h).

At low magnification (Fig. 1(a-d), Columns 1,2 in Table S2, Supplement 1), the spherical or elongated structures show pointillistic color patterns in both bright-field and dark-field imaging. In bright-field, specular reflections and diffuse scattering contribute to the image, while dark-field imaging records only diffusely scattered light. The sporothecae, respectively the peridia enclosing them, appeared wrinkled and had similar hues in both imaging modes, likely due to non-directional scattering.

To investigate the colors further, we performed high-magnification bright-field microscopy. Most investigated species (Fig. 1(e-h), Column 3 in Table S2) showed multicolored wrinkled surfaces. Wrinkles of the surface were visible as dark lines, while extended dark brown or orange areas indicated a ruptured peridium that exposed the spores inside the sporotheca. These spores occasionally fell out onto the peridium. In high-magnification dark-field images (Column 4 in Supplement 1, Table S2), only the surface wrinkles showed rainbow-like colors, suggesting that the curved surfaces created mirror angles reflecting light into the collected scattering angles determined by the numerical aperture of the objective.

To assess the spectral properties of each species, we recorded bright-field reflectance spectra of differently colored spots on the peridia. The majority of specimens produced reflectance spectra with broad peaks throughout the visible spectrum and a reflectance below 0.5, see

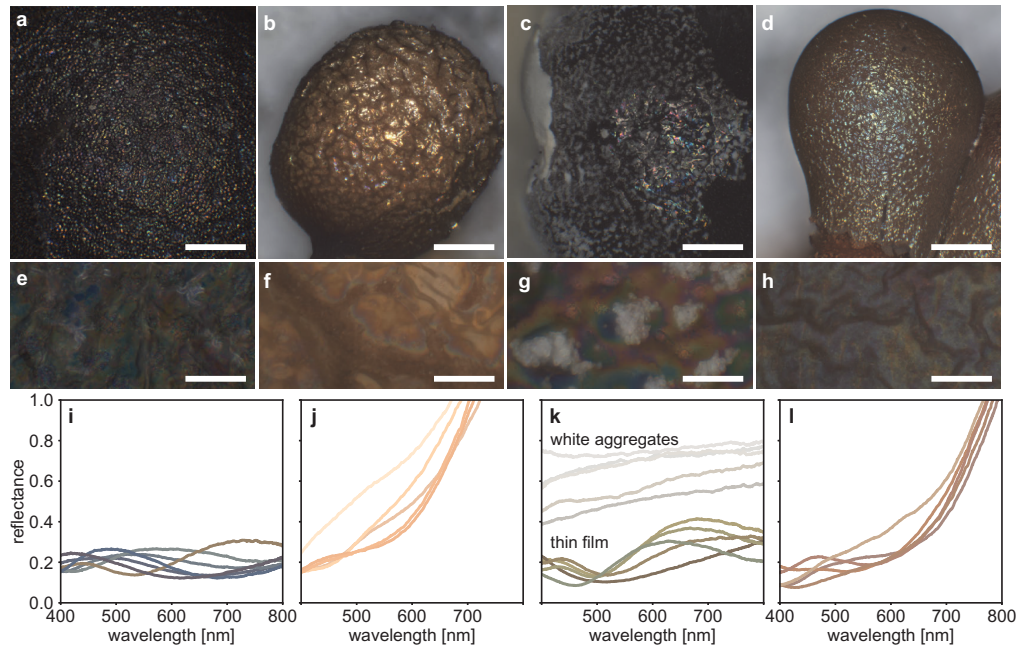


Fig. 1. Bright-field optical micrographs of sporothecae of **a,e** *Lamproderma cristatum*, **b,f** *Cribraria argillacea*, **c,g** *Diderma meyerae* and **d,h** *Metatrachia vesparium*. **i-l** Reflectance spectra of sporothecae peridia for $N = 5 - 6$ spots measured on each sample, normalized to a white diffuser, and colored as estimated from the spectral shape. Scale bars a-d 200 μm , e-h 20 μm

Fig. 1(i,k). Column 5 in Supplement 1, Table S2 summarizes the reflectance curves measured for all specimens, which were strongly reminiscent of thin film interference effects in intensity and shape [1,31,43]. For some specimens, the typical thin film spectra seemed superimposed on an increasing reflectance above 600 nm (see Fig. 1(j,l), Supplement 1, Table S2). A reflectance higher than one results from the normalization to a white diffuser, a suitable reference for most of the low-intensity reflecting, wrinkled fruit body surfaces and usually employed to measure diffusely reflecting samples. These spectral differences, however, were likely related to pigment content variations in the peridia and the spores below the peridia, which appeared either black, dark brown, or orange according to their classification as dark-spored and bright-spored species.

We analyzed the pigment content in the peridia of two specimens, one dark-spored species (*L. cristatum*, low reflectance) and one bright-spored species (*C. argillacea*, high long-wavelength reflectance), using transmission measurements. The in-air and in-oil transmittance of *L. cristatum* (Fig. 2(a)) peridia was higher than those of *C. argillacea* (Fig. 2(b)) and both curves showed a decreasing transmittance towards shorter wavelengths, typical for e.g. melanin pigments creating orange or brown coloration, which are found in many animals but also myxomycetes [39]. Assuming equal thicknesses, this would indicate a higher pigment content in *C. argillacea*. The average thickness of *C. argillacea* peridia of 100(20) nm is even less than the 270(50) nm of *L. cristatum*, thus confirming a higher pigment content in the first (Supplement 1, Table S3). Using the Kramers-Kronig relations [44,45] allowed calculating a complex refractive index of the peridia assuming that their main component is cellulose as suggested by Martin [46]. Note that experimental data on the exact chemical composition of the peridium and spores are scarce and not unequivocal [28,47,48], yet differences in the exact composition would not change the optical results as most biomaterials have rather similar refractive indices 1.5–1.6 [49]. Figure 2(c)

shows that the real part of the refractive index n_r of the two species' peridium is within the range reported for most biopolymers. The difference in the imaginary part of the refractive index (n_k) arises from the different pigment content as interference effects are suppressed by the surrounding oil. Neglecting negligible intensity changes from defect scattering and intensity changes due to local thickness variations, we relate spectral variations in the thickness-normalized absorption magnitudes, respectively n_k , to variations in pigment composition given the extensive literature on pigments found in myxomycetes [35–39].

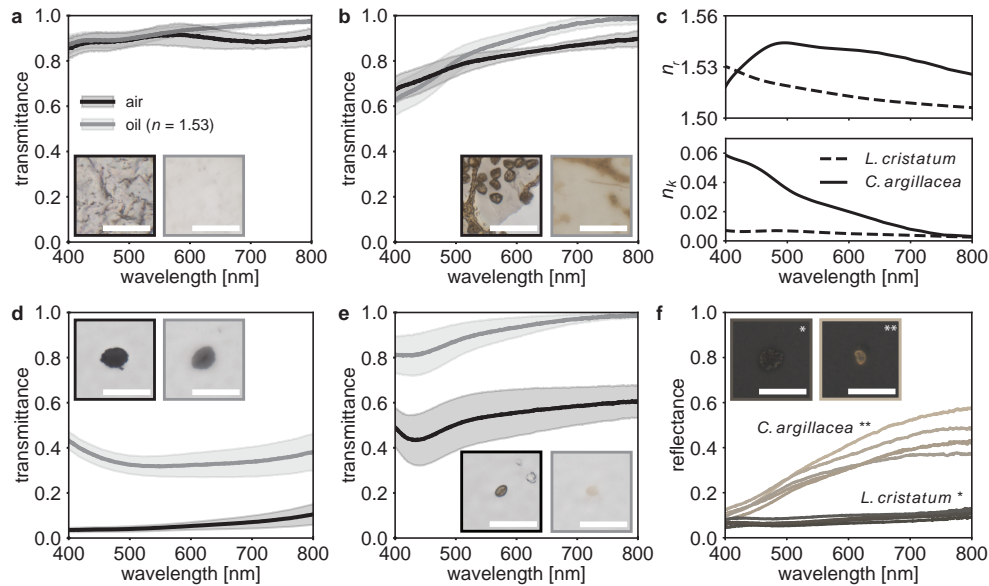


Fig. 2. Pigment analysis of the peridia and spores of *Lamproderma cristatum* and *Cribraria argillacea*. **a,b** Transmittance of peridia in *L. cristatum* (a) and *C. argillacea* (b) in air (black) and oil of refractive index $n = 1.53$ (grey). Continuous lines are averages of $N = 10$ measurements, shaded areas indicate the corresponding standard deviation. Insets: Optical micrographs in transmission mode for samples on glass slides in the air (black frame) and immersed in oil (grey frame). **c** Complex refractive indices $n = n_r + in_k$ calculated with the Kramers-Kronig relations from average transmittance spectra of *L. cristatum* and *C. argillacea*. **d,e** Transmittance of the spores ($N = 5$) in *L. cristatum* (d) and *C. argillacea* (e) in air (black) and oil ($n = 1.53$, grey). Optical transmission micrographs of spores in air and oil as in a,b. **f** Reflectance spectra of individual spores ($N = 5$) of *L. cristatum* (*) and *C. argillacea* (**) on carbon tape, normalized to a white diffuser. Insets: Optical reflection micrographs in reflectance mode of spores on carbon tape. Scale bars a,b,d,e,f 25 μm .

To assess the influence of spore pigmentation on the reflectance of the intact peridium covering the spores, we characterized individual spores of *L. cristatum* and *C. argillacea* with reflectance and transmittance measurements. Figure 2(d-f) summarizes the results of the dark and orange spores of *L. cristatum* and *C. argillacea*, respectively. The insets in Fig. 2(d-f) show spores in reflection (f) and transmission mode in air and oil (d,e). As seen in Fig. 2(d), the intensity of light transmitted through the dark spores of *L. cristatum* was low (<0.1) and increased to about 0.4 after oil immersion ($n = 1.53$). Orange spores of *C. argillacea* appeared beige in transmission mode, with transmitted intensities of about 0.5 in air and a minimum transmittance of about 0.8 after oil immersion (Fig. 2(e)). With the spore transmittances not normalized to the spore thickness, a *C. argillacea* spore thus absorbs less light than a *L. cristatum* spore and likely contains different pigments than *L. cristatum* spores due to the differently shaped in-oil transmittance. To directly

estimate the impact of varying spore pigmentation on the overall reflectance spectrum of the intact peridia, we recorded reflectance spectra of the two spore types. As shown in Fig. 2(f), *L. cristatum* spores (marked with *) reflected about 10% of the incoming light throughout the visible spectrum. The reflectance of individual orange *C. argillacea* spores (marked with **) increased from 10% to about 50% compared to a white diffuser for long wavelengths. The increase in reflectance for increasing wavelengths observed in bright-spored species with typical thin film peridia is thus explicable with a substantial pigmentary contribution from the underlying spores. Conversely, in dark-spored species, we expect black spores to absorb most of the light transmitted through the peridium and thus create a roughly constant background. In the case of *L. cristatum*, the background signal from the dark spores amounted to about 0.1 reflectance.

Four species, *Diderma meyerae*, *Didymium difforme*, *Lamproderma pseudomaculatum* and *Metatrichia vesparium*, showed peridium morphologies different from simple thin film structures. In all cases, white elements were observed near the peridium, which differed in geometry and position.

The peridium comprised two layers in *D. meyerae*. The outer layer formed an about 20 μm continuous white layer of aggregated spheres (visible in Supplement 1, Table S2, H1,2,6). The inner layer is a membrane covered with aggregates of spheres sparsely distributed over the entire inner peridium surface (see Fig. 1(c,g)). Similar to *D. meyerae*, the peridia of *D. difforme* were partially covered by a continuous white layer, and crystalline flakes sparsely covered the peridium in exposed areas (see Table S2, I7). The peridium of *L. pseudomaculatum* was decorated with white, cylindrical elements (Table S2, P1,7) that did not form a continuous layer. Previous studies related these deposits on or in myxomycetes peridia to lime or various other calcium compounds [28,50–52]. Investigating the formation of these deposits was outside the scope of this study. Their presence as white-reflecting, polydisperse aggregates of spheres in *D. meyerae* (see Fig. 1(k), white aggregates) averages with the optical signal produced by the underlying thin film (see Fig. 1(k), thin film) and renders the macroscopic appearance of the peridia a shallow gray. For the investigated samples of *D. difforme* and *L. pseudomaculatum*, the small amounts of white coverage and flakes or cylinders, respectively, did not influence its macroscopic appearance and were thus not studied in more detail. They could result in a grey appearance for an intact white layer as outer peridium.

In contrast to the peridia of *D. meyerae*, *D. difforme* and *L. pseudomaculatum*, which carried visible calcium-rich deposits, intact peridia of *M. vesparium* sporothecae, shown in Fig. 1(d,h), appeared as simple thin film structures and produced a high long-wavelength reflectance (Fig. 1(l)). Surprisingly, ruptured peridia revealed an about 20 μm to 40 μm thick, bright layer packed between two thin films (Fig. 3(a)).

The peridium appeared opaque when immersed in refractive-index matching oil, as seen in Fig. 3(c). The thin film on top showed similar transparency as the peridium in *C. argillacea* (see Fig. 3(b), compare Fig. 2). We hypothesized two possible origins of the low transparency of the entire peridium: a) the bottom thin film is highly pigmented, and b) the refractive index matching oil did not entirely suppress potential interference effects. In either case, very low amounts of light reach the spores in *M. vesparium* sporothecae. This, in turn, indicates that the high reflectance for long wavelengths cannot be caused by the optical signal of the pigmented, orange-appearing spores inside *M. vesparium* sporothecae.

In short, optical characterization showed that while pigmentary coloration of peridia and spores varies among myxomycetes, the structural colors observed in myxomycetes are very similar across species. Therefore, structural colors do not allow unambiguous identification as a standalone parameter in myxomycetes. In all species, the structural coloration is reminiscent of thin film interference. One species, *M. vesparium*, showed exceptionally minimal peridium transmittance and a complex peridium morphology, which we subsequently investigated in detail using scanning electron microscopy.

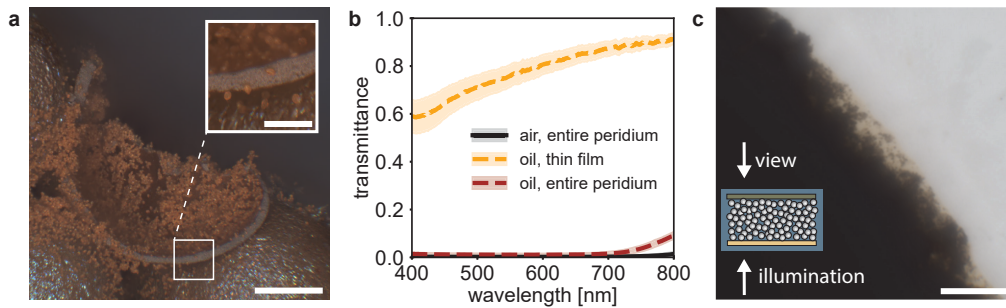


Fig. 3. **a** Optical micrograph of the compound peridium in *Metatrachia vesparium* sporothecae in reflection imaging mode. Inset: Close-up micrograph of the bright layer. **b** Transmittance spectra of the compound layer (entire peridium) in the air (black) and the compound layer and outer film only in refractive index matching oil with $n = 1.53$ (red and orange, respectively). **c** Optical micrograph of the compound peridium immersed in oil ($n = 1.53$) in transmission mode. The bright areas are standalone outer thin film pieces. Inset: Sketch of the compound layer with inner (dark green) and outer (bright yellow) film and the bright granular layer in between in oil (blue). Arrows indicate the viewing and illumination directions. Scale bars a 200 μm , inset a 50 μm , c 20 μm

2.2. Ultrastructural analysis of the fruit bodies uncovers thin film peridia and reveals complex calcium decorated compound peridia

We characterized the peridium ultrastructure with scanning electron microscopy to confirm that the iridescent colors observed for peridia at high magnification result from thin film interference.

All sporothecae featured a wrinkled peridium (see Columns 6,7 in [Supplement 1](#), Table S2) that seemed morphologically related to the spore packing inside the sporothecae. The fragile structures partly cracked during sample preparation, which allowed for imaging of fractured peridia and confirmed the preliminary explanation that a thin film layer as shown in Fig. 4(g,h) is responsible for the angle-dependent coloration at high magnification (see Column 7 in Table S2). Measured film thicknesses ranged from 70 nm to 670 nm (see Table S3), which is comparable to what has been reported for *Diachea leucopodia* sporothecae [26,27] and is in line with theoretical predictions for the optical response of thin films in other natural systems [1,31,43]. The film thickness locally varies, which results in a broadening and shifting of the reflectance peaks compared to an ideal reflector [53,54].

The wrinkles in the peridia form three-dimensional patterns with periodicities of about 1.9 μm to 41.0 μm and total height variations of 0.3 μm to 6.9 μm (see [Supplement 1](#), Figure S1, Table S3). These variations are mostly macro-scale and larger than the coherence length of visible light, which is about 1.2 μm for sunlight [55]. Therefore, the wrinkles were not expected to alter the optical response significantly.

In *D. meyeriae*, the sphere aggregates on the inner peridium, shown in Fig. 4(a), were loosely attached to the latter as individual spheres came off during sample preparation. Further, a single drop of water on the sample was sufficient to partially wash off the aggregates, and incompletely dissolve the filled spheres (Fig. 4(d)). EDXS line scan measurements of the spheres with an average diameter of 1130(285) nm ($N = 107$), one is displayed in Fig. 4(b), confirmed the common identification for *Physarales* as a calcium compound [28,50,51,56].

Ultrastructural analysis of the *M. vesparium* peridium shed light on the morphology of the bright layer between thin films observed in the light microscope. In the bright layer, visible in Fig. 4(c), shells of diameter 580(57) nm ($N = 64$) and shell thickness 89(13) nm ($N = 24$) are densely packed. Individual shells, one broken, others intact, are displayed in Fig. 4(f). No particular periodicity or symmetry was observable in their arrangement from SEM images, and a

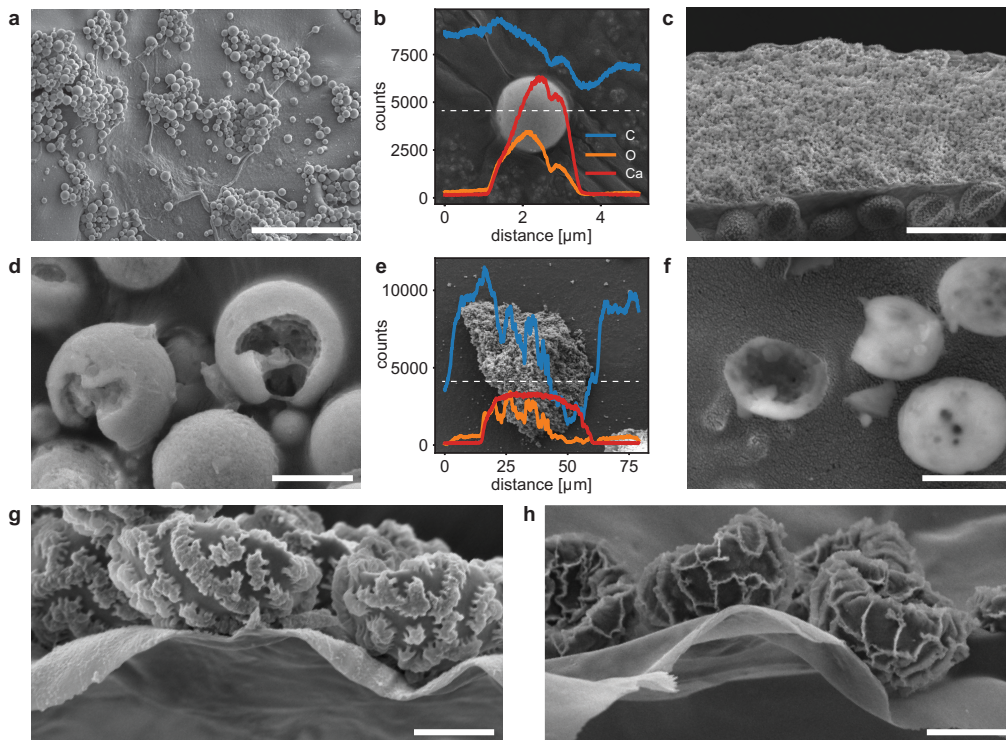


Fig. 4. **a** Scanning electron microscopy image of the inner peridium in *Diderma meyerae* shows the sphere aggregates. The spheres were easily washed off with water and seemed to have partially dissolved (**d**). **b,e** EDXS measurements of an individual sphere in *D. meyerae* (**b**) and an assembly of shells in *Metatrachia vesparium* (**e**). Horizontal line scans were performed along the dashed white lines in the overlaid sample areas. Curves indicate the distribution of carbon (C, blue), oxygen (O, orange), and calcium (Ca, red) content in absolute counts along that line (image scaled to the scale of the plot). **c** SEM image of the compound peridium in *M. vesparium* that features two thin films enclosing a granular structure. **f** Close-up SEM image of individual elements revealed the bright layer's elements as shells. **g,h** SEM images of the peridia thin films of *Lamproderma cristatum* and *Diachea cylindrica*, with attached structured spores. Scale bars **a,c** 20 μm , **d** 1 μm , **f** 500 nm, **g,h** 5 μm .

three-dimensional analysis was outside the scope of this work. However, the size of the shells fell into the scale where interference effects in the visible spectrum are expected, which motivated further analysis of this structure using optical modeling (see Section 2.3). The composition analysis of the shells using EDXS, summarized in Fig. 4(e), suggested a similar calcium compound as in the spheres found in *D. meyerae* despite their different morphologies. These results are consistent with those obtained by Nelson et al. [52], who detected calcium concentrations in sporophores of *M. vesparium* at levels as high as in some *Physarales* representatives where calcium compounds are common [28,50,51].

Given this structural insight, for in-oil transmittance measurements, one could not expect the refractive index matching oil with $n = 1.53$ to penetrate the shells and to suppress interference effects due to the refractive index mismatch completely. Under the assumption that the two thin films outside the bright layer are similar in composition and thickness, an incomplete immersion of a photonic structure likely explains the very low in-oil transmittance.

SEM also allowed for additional insight into the spore morphologies, which are visible in Fig. 4(g,h) and Column 7 in Supplement 1, Table S2 as dimpled spheres with distinct spore

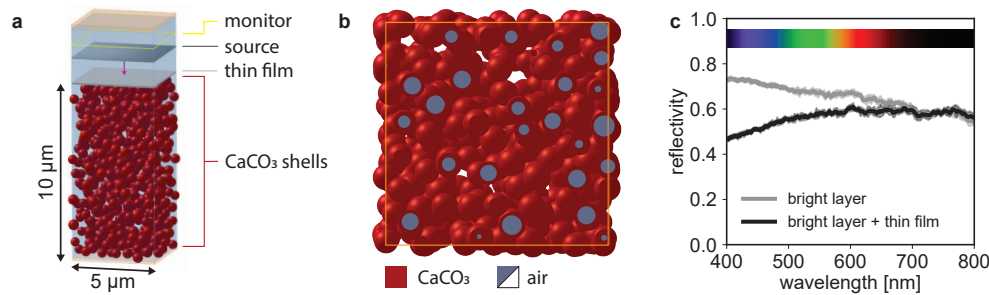


Fig. 5. **a** View of a generated structure and the simulation environment. Shells are drawn in red, and the thin film in grey. Dark grey and yellow rectangles above the thin film represent the source and monitor, respectively. The purple arrows indicates the source injection direction. **b** Top-view cross-section of the shell assembly. Grey circles represent the air-filled interior of the shells drawn in red, the surrounding air is white. The simulation box is framed in orange. **c** Simulated reflectivity of the shell assembly (grey) and the shell assembly covered with a pigmented thin film (black). The colored band indicates the visible spectrum.

surface patterns. The dimpling is a result of the drying process since the critical point drying technique was not applied (see e.g. [57]). While not a standalone parameter, these so-called spore ornamental elements are a major aspect of taxonomic and phylogenetic studies and are widely used as important characters distinguishing species and species groups [28,58,59].

2.3. Optical simulations of the densely-packed calcified shells in *Metatrachia vesparium* attest a high reflectance to the structure

The reflectance of the compound peridium in *M. vesparium* did not exceed the characteristics of other peridia despite its more complex morphology. We performed optical simulations of the compound peridium to unveil the bright layer's optical (ir)relevance.

The shell assembly mimicking the bright layer with an assumed average refractive index $n = 1.572 + i \cdot 10^{-5}$ (see Section 5) behaved as a broad-band reflector throughout the visible spectrum with intensities above 0.5 (grey line in Fig. 5(c)), as expected for a random assembly of shells varying in size [8,60]. This result implies that only a small fraction of the incoming visible light will reach the bottom thin film. Assuming the bottom film also contains pigments, the light reaching the sporothecae's inside will be negligible, confirmed by transmittance measurements (Fig. 3(b)). More importantly, this fraction will be much smaller than in all other specimens investigated in this work.

Expanding the structure by adding a pigmented, 100 nm thick film above the shell assembly unsurprisingly decreased the reflectivity towards shorter wavelengths. The resulting spectrum followed the trend of the measured reflectance with increasing intensity for longer wavelengths but did not show any spectral variation at short wavelengths (compare Fig. 1(l)). This can be explained with the different film thicknesses resulting from our approximation of the measured transmittance of the upper, 550(30) nm thick film in *M. vesparium* with the 100(20) nm thick peridium in *C. argillacea*. Further, different normalizations in the simulation and the microscope did not allow for comparing absolute intensities. Increasing the thickness of the scattering layer will further increase the maximum reflectivity as scattering will increase while increasing the top film thickness will result in a higher short-wavelength absorption.

3. Discussion

By combining optical and ultrastructural characterization of 22 myxomycetes species spanning the entire phylogenetic diversity of the group, we here related the observed structural color in

multicolored peridia to thin film interference. The optical appearance of myxomycete fruit bodies is further altered by pigmentary content in the peridium or the underlying spores and the presence of white calcium compounds in the vicinity of the peridium.

These calcium-rich deposits were either on the outside of the thin film layer (*Diderma meyerae*, *Didymium difforme*, *Lamproderma pseudomaculatum*) or within a compound peridial layer (*Metatrachia vesparium*). In the framework of biomineralization of photonic structures, the calcium-rich white structures in some myxomycete species add to a variety of CaCO_3 (calcium carbonate) structures that occur in living organisms [56,61–64]. Photonic structures based on CaCO_3 have been described primarily in the context of marine environments, including the well-known iridescent nacre in the shells of mollusks [65,66]. With structures ranging from lamellar calcite producing bright blue in blue-rayed limpets [64] to regular arrays in brittlestar and holococcolithophores [67,68], acting as microlenses or UV reflectors, respectively, CaCO_3 -based marine photonic structures cover a parameter space exceeding the scope of this paper. CaCO_3 has also found its way into technological applications in biophotonics and radiative cooling [69,70]. Given the optical properties of the white layer composed of calcium-rich shells in *M. vesparium*, understanding its formation may open the door to future applications of CaCO_3 -based materials.

In species without calcium-rich deposits, we observed two different optical appearances in myxomycetes fruit bodies, with either low or high peak reflectivity. Both types can be understood considering the interplay of thin film interference with pigmentary absorption of the underlying spores and within the peridium. Light interference at the pigmented peridium produced reflectance spectra with one or several peaks in the visible. The peridium thickness governs the perceived color and color variability with changing viewing angle as a function of the visual receptor response [1,43,71]. Translating the reflectance spectra to the spectral sensitivity of human visual receptors, one obtains RGB values as a color chart [71,72] shown in Supplement 1, Fig. S2. At normal incidence, peridia films thinner than 50 nm do not show colors in the visible range. For peridia with local thickness of about 60 nm to 110 nm, as observed in e.g. *Cribraria argillacea*, *Comatracha fusiformis*, *Licea kleistobolus* and *Meriderma spinulosporum* (see Table S3, Table S2, A,K,C,U, respectively), a silvery or golden shine is expected when considering the mostly flat or broad reflectance spectrum combined with the specular reflection from each face of the wrinkled peridium [31,32,73]. Pure spectral colors are seen for peridium thin films of thickness 150 nm to 450 nm. Peridia with a thin film thickness above 450 nm appear in dull, more washed-out colors due to the reflectance spectra featuring several peaks in the visible wavelength range.

Most incident light is transmitted when illuminating the peridium at normal incidence (see Fig. 2). Consequently, the optical appearance of the spores contributes significantly to the observed color of the intact peridium with either bright or dark spores, depending on the lineage [41,42]. The observed fruit body color thus depends on the spore pigmentation: in species with bright spores, i.e., *Cribraria argillacea*, *Licea kleistobolus*, *Arcyria versicolor*, *Calomyxa metallica*, and *Dianema* spp. (and not in italic), the color of the spores contributes to the high reflectance in the long-wavelength spectrum as a function of the pigmentary absorption in the peridium (Supplement 1, Table S2, Column 5, A–E). Species with dark spores (all other species studied here) result in spectra of peridia with overall low reflectance as most of the transmitted intensity is absorbed by the spores.

In four species, *D. meyerae*, *D. difforme*, *L. pseudomaculatum* and *M. vesparium*, we found white, calcium-enriched deposits on the outside or inside of the otherwise similar peridium, which is common in some groups of myxomycetes [50–52]. In *D. meyerae* and *D. difforme*, the deposits are found as an additional layer on the inner peridium in the form of calcium-rich, densely packed or sparsely distributed spheres and flakes, respectively. Peridia of *L. pseudomaculatum* are decorated with cylinders, while *M. vesparium* forms an about 20 μm to 40 μm thick layer of calcium-rich shells between two thin films. It will be interesting to investigate the formation or

crystallinity of those deposits in the future, and their presence and distribution in the peridium raise interesting questions about their optical or biological relevance. The white layers in *D. meyeriae*, *D. difforme* and *M. vesparium* reduce transmittance to the spores regardless of their exact position. It remains to be clarified whether these lime morphologies potentially evolved for this optical function of reducing light exposure of the spores. Conversely, the calcium deposits might be by-products of the organisms' metabolism and related to the local soil composition. This should be considered in the light of the different morphologies. It would be interesting to study a possible correlation between the presence of such a reflecting layer and the species' habitat. Considering the water solubility of calcium, the compound layer morphology in *M. vesparium* appears more resistant to dissolution, leading to the hypothesis that it may serve a distinct purpose, e.g., optical, thermal, or mechanical.

Previous work on structural color in slime molds was restricted to one species, *Diachea leucopodia*, and mainly focused on a qualitative understanding of the pointillistic appearance of the peridium [26,27]. In optical simulations of the peridium in *D. leucopodia*, refractive indices of up to $n = 2$ were assumed [27], which are comparably high for biological, and especially cellulose-based, samples [15,74]. Our work adds a quantitative assessment of the colors observed in myxomycetes fruit bodies to the scarce literature on colors in myxomycetes and fills a gap in determining the refractive index of the peridium (see Fig. 2). While earlier analyses were restricted to the optical properties of the peridium, we here conclusively show that the fruit body coloration is the result of structural and pigmentary color.

Do the peridial colors serve a biological purpose? Previous work investigating the function of the pointillistic appearance questioned the biological relevance of structural colors in myxomycetes [26,27], and our study agrees with this. As spore propagation in myxomycetes is airflow-based [58,75], it seems unlikely that the structural coloration of the peridium serves a direct biological purpose. In contrast to flowers, where the visual appearance of petals is key for attracting pollinating insects [14,76], myxomycetes do not depend on the visual perception of peridium colors by a distributing species. Therefore, the colors more likely arise as a by-product during sporothecae maturation. As the hydrated peridium dries out, it loses its protective function and eventually breaks to enable spore release. As the thickness decreases, the underlying spores shape its local curvature. To test if the color arises during this maturation process, it would be interesting to perform a time-dependent growth study of the peridium and eventually clarify the structural color's (ir)relevance in myxomycetes.

4. Conclusion

Through combined optical and ultrastructural examinations of the peridia across 22 distinct myxomycetes species, we showed that the intricate pointillistic appearance of the fruit bodies, evident at high magnifications, is largely attributed to thin film interference occurring at the peridium. The macroscopic visual appearance of these fruit bodies is a combination of pigment absorption in the spores and peridia, combined with the aforementioned thin film interference. While the prevalent occurrence of structural coloration in myxomycetes might not have a direct visual significance, it offers a foundational understanding of the coloration mechanisms in fruit bodies, likely motivating future taxonomic studies of myxomycetes.

5. Experimental section

5.1. Specimens

We studied dried sporothecae of 22 myxomycete species ($N = 1 - 10$ per species) (Supplement 1, Table S1) from collection sites indicated in Fig. 6.

We selected the species so that they represent the two major phylogenetic lineages, light-spores and dark-spored groups [41,42] indicated by open and filled circles in Table S2 and most orders

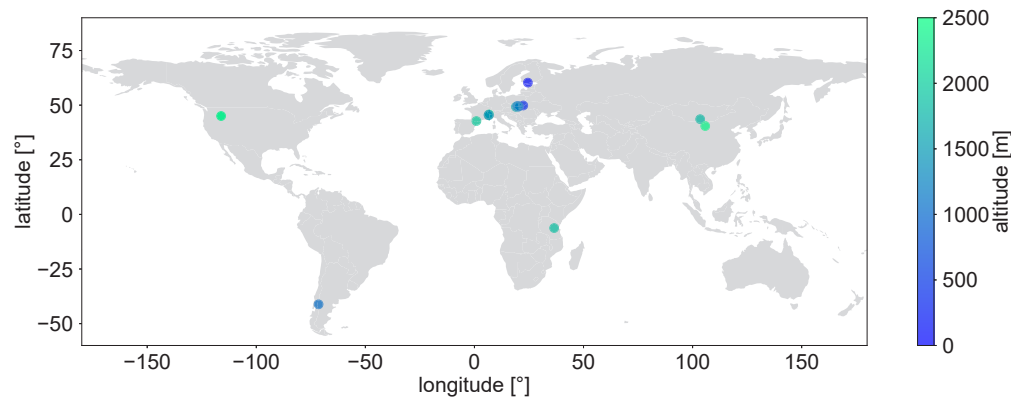


Fig. 6. Geographical origins of the samples investigated in this study, including the color-coded altitude of the collection area.

belong to the subclasses Myxogasteromycetidae and Stemonitomycetidae [77] (Supplement 1, Table S1 lists all specimens with their order, family, and genus). Taxonomy and nomenclature follow the newest taxonomic revisions [77–79]. All specimens are deposited in the herbarium of the W. Szafer Institute of Botany, Polish Academy of Sciences (KRAM).

5.2. Optical characterization

Reflectance micrographs of the peridium in the samples were recorded with an Axio Scope.A1 (Zeiss, Germany) light microscope connected to a Xenon lamp (ThorLabs, SLS401) in bright-field and dark-field with objectives of magnification 10x ($NA = 0.25$, EC Epiplan-Neofluar), 20x ($NA = 0.6$, EC Epiplan-Apochromat) and 100x ($NA = 0.9$, EC Epiplan-Neofluar). We used a white diffuser for white balance calibration (Labsphere, Spectralon USRS-99-010).

Reflectance microspectrophotometry (MSP) spectra of differently colored spots on each sample ($N = 5 - 6$) were recorded with the 100x objective by placing an optical fiber (OceanOptics, QP230-1-XRS) in a plane confocal to the image plane that was connected to a spectrometer (OceanOptics, QEPRO-VIS-NIR). Samples were placed onto a patch of double-sided carbon tape (Micro to Nano). The setup with a resulting measurement spot of 2 μm in diameter was calibrated with the white diffuser as a white reference and a tilted glass slide covered with carbon tape without any sample as the dark reference to account for internal reflections in the optical setup. Reflectance spectra were converted to RGB values with the Python package *colour-science*.

Transmission spectra of peridia obtained from ruptured specimens were recorded with the 100x objective. Spectra were recorded of specimens on a glass slide in air first and subsequently of the identical specimens immersed in a refractive-index oil ($n = 1.53$, Cargille Series A, using a cover slip on top) matching the refractive index of dried cellulose [15,74]. Empty regions on the glass slides served as bright reference and white standard. The dark reference was recorded with the illumination source blocked. A comparison of the transmittance in air and oil allowed for a qualitative pigment content analysis. The weaker the difference in transmittance, the lower the structural component of the observed color in air, hence, the higher the pigment content.

Using the Kramers-Kronig-relationship between a material's absorbance A , which we calculated via $A = -\log_{10}(T)$ from the in-oil transmittance T and its refractive index, we estimated the complex refractive index of the specimens' peridia [44].

5.3. Ultrastructural characterization

We performed ultrastructural characterization on samples mounted on double-sided carbon tape with a Tescan Mira3 LM field-emission scanning electron microscope (SEM). To prevent

charging artifacts, the samples were sputtered with an about 4 nm thick gold layer (Cressington 208HR, UK) and imaged at 5 kV. Geometrical parameters were measured in SEM images and averaged ($N = 3 - 13$).

Energy-dispersive X-ray spectroscopy (EDXS) was performed in the SEM at 20 kV to study material composition. Data were recorded and analyzed with Aztec software, and line spectra were subsequently exported and plotted with Python using *matplotlib*.

5.4. Full-wave optical simulations

For one specimen, *Metatrichia vesparium*, optical simulations in three dimensions were performed with the finite-difference time-domain (FDTD) method using the software Lumerical (v. 2023R1.3), a commercial FDTD solver. Periodic boundaries enclosed the structure in plane and perfectly matched layers (PMLs) along the illumination axis. The structure was illuminated with a broad-band plane wave source from above, where a frequency domain power monitor above the source measured the reflectivity of the structure within the wavelength range of 300 nm to 1000 nm. Simulations were performed with a mesh size of 20 nm for polarization angles 0° and 90° and averaged to approximate unpolarized illumination.

The in SEM images random appearing assembly of hollow spheres in *M. vesparium* peridia was approximated with a collection of shells designed to match the experimental values in diameter, using a distribution between 520 nm and 640 nm, and shell thickness of 89 nm, matching the experimental average shell thickness. The shells were assigned the average refractive index reported for CaCO_3 ($n = 1.572 + i10^{-5}$, [80]), without accounting for birefringence, and distributed using the uniform random particle distribution function in Lumerical to approximate their seemingly random arrangement. The number of elements was set to 1000, higher than the actual number of spheres placed which was usually between 550 and 650 depending on the seed, to obtain a dense shell packing in a $5 \times 5 \times 10 \mu\text{m}^3$ volume.

For a qualitative understanding of the assembly, its height was chosen as about a third of the bright layer's thickness, which was also motivated by computational limitations. We simulated 10 different random assemblies and averaged the results to decrease the influence of any particular configuration.

In additional simulations, a slab of 100 nm thickness mimicked the outer thin film above the shell assembly, while we did not consider the bottom thin film here. The absolute transmittance of the outer film in *M. vesparium* was identified as pigmented similarly to *C. argillacea* (see Fig. 2(b), Fig. 4(b)). Therefore, we used the respective film thickness and assigned the calculated complex refractive index of *C. argillacea* to the slab, thus taking absorption in the slab into account. A generated structure, a cross-section and the simulation setup are shown in Fig. 5(a,b).

The visible spectra indicator in Fig. 5(c), was generated with the Python module *colour-science*.

Funding. Adolphe Merkle Foundation; HORIZON EUROPE European Research Council (833895); Schweizerischer Nationalfonds zur Förderung der Wissenschaftlichen Forschung (NCCR Bio-inspired Materials); Statutory funds of the Institute of Botany, Polish Academy of Sciences.

Acknowledgment. We thank V. Vogler-Neuling for helpful discussions.

Disclosures. The authors declare no conflicts of interest.

Data availability. The data supporting this study's findings are available as Zenodo open repository at [81].

Supplemental document. See [Supplement 1](#) for supporting content.

References

1. S. Kinoshita, *Structural colors in the realm of nature* (World Scientific, 2008).
2. E. Bermúdez-Ureña, C. Kilchoer, N. P. Lord, *et al.*, "Structural diversity with varying disorder enables the multicolored display in the longhorn beetle *Sulawesiella rafaetae*," *iScience* **23**(7), 101339 (2020).
3. V. Bauernfeind, K. Djeghdi, I. Gunkel, *et al.*, "Photonic amorphous I-WP-like networks create angle-independent colors in *Sternotomis virescens* longhorn beetles," *Adv. Func. Mater.* **2302720** (2023).

4. V. Hwang, A. B. Stephenson, S. Magkiriadou, *et al.*, “Effects of multiple scattering on angle-independent structural color in disordered colloidal materials,” *Phys. Rev. E* **101**(1), 012614 (2020).
5. B. D. Wilts, X. Sheng, M. Holler, *et al.*, “Evolutionary-optimized photonic network structure in white beetle wing scales,” *Adv. Mater.* **30**(19), 1702057 (2018).
6. S. R. Sellers, W. Man, S. Sahba, *et al.*, “Local self-uniformity in photonic networks,” *Nat. Commun.* **8**(1), 14439 (2017).
7. J. S. Haataja, G. Jacucci, T. G. Parton, *et al.*, “Topological invariance in whiteness optimisation,” *Commun. Phys.* **6**(1), 137 (2023).
8. G. Jacucci, L. Schertel, Y. Zhang, *et al.*, “Light management with natural materials: from whiteness to transparency,” *Adv. Mater.* **33**(28), 2001215 (2021).
9. S. Berthier, *Iridescence* (Springer, 2007).
10. M. D. Shawkey and L. D’Alba, “Interactions between colour-producing mechanisms and their effects on the integumentary colour palette,” *Philos. Trans. R. Soc., B* **372**(1724), 20160536 (2017).
11. J. Tinbergen, B. D. Wilts, and D. G. Stavenga, “Spectral tuning of Amazon parrot feather coloration by psittacofulvin pigments and spongy structures,” *J. Exp. Biol.* **216**(23), 4358–4364 (2013).
12. M. Xiao, M. D. Shawkey, and A. Dhinojwala, “Bioinspired melanin-based optically active materials,” *Adv. Opt. Mater.* **8**(19), 2000932 (2020).
13. T. Sai, L. S. Froufe-Pérez, F. Scheffold, *et al.*, “Structural color from pigment-loaded nanostructures,” *Soft Matter* (2023).
14. E. Moyroud, T. Wenzel, R. Middleton, *et al.*, “Disorder in convergent floral nanostructures enhances signalling to bees,” *Nature* **550**(7677), 469–474 (2017).
15. S. Vignolini, P. J. Rudall, A. V. Rowland, *et al.*, “Pointillist structural color in *Polinia* fruit,” *Proc. Natl. Acad. Sci.* **109**(39), 15712–15715 (2012).
16. C. J. Chandler, B. D. Wilts, J. Brodie, *et al.*, “Structural color in marine algae,” *Adv. Opt. Mater.* **5**(5), 1600646 (2017).
17. R. Middleton, M. Sinnott-Armstrong, Y. Ogawa, *et al.*, “*Viburnum tinus* fruits use lipids to produce metallic blue structural color,” *Curr. Biol.* **30**(19), 3804–3810.e2 (2020).
18. G. Strout, S. D. Russell, D. P. Pulsifer, *et al.*, “Silica nanoparticles aid in structural leaf coloration in the Malaysian tropical rainforest understorey herb *Mapania caudata*,” *Ann. Bot.* **112**(6), 1141–1148 (2013).
19. L. Feng, Y. Zhang, M. Li, *et al.*, “The structural color of red rose petals and their duplicates,” *Langmuir* **26**(18), 14885–14888 (2010).
20. B. D. Wilts, P. J. Rudall, E. Moyroud, *et al.*, “Ultrastructure and optics of the prism-like petal epidermal cells of *Eschscholzia californica* (California poppy),” *New Phytol.* **219**(3), 1124–1133 (2018).
21. M. J. Christenhusz and J. W. Byng, “The number of known plants species in the world and its annual increase,” *Phytotaxa* **261**(3), 201–217 (2016).
22. D. L. Hawksworth and R. Lücking, “Fungal diversity revisited: 2.2 to 3.8 million species,” *Microbiol. Spectrum* **5**(4), 1128 (2017).
23. J. Brodie, C. J. Ingham, and S. Vignolini, “Does structural color exist in true fungi?” *J. Fungi* **7**(2), 141 (2021).
24. G. Martin and C. Alexopoulos, *The myxomycetes* (University of Iowa Press, Iowa City, IA, USA, 1969).
25. J. M. Archibald, A. G. Simpson, C. H. Slamovits, *et al.*, *Handbook of the Protists* (Springer International Publishing Cham, Switzerland, 2017).
26. M. Inchaussandague, D. Skigin, C. Carmaran, *et al.*, “Structural color in Myxomycetes,” *Opt. Express* **18**(15), 16055–16063 (2010).
27. A. Dolinko, D. Skigin, M. Inchaussandague, *et al.*, “Photonic simulation method applied to the study of structural color in Myxomycetes,” *Opt. Express* **20**(14), 15139–15148 (2012).
28. J. Clark and E. Haskins, “Sporophore morphology and development in the myxomycetes,” *Mycosphere* **5**(1), 153–170 (2014).
29. D. G. Stavenga, A. Matsushita, K. Arikawa, *et al.*, “Glass scales on the wing of the swordtail butterfly *Graphium sarpedon* act as thin film polarizing reflectors,” *J. Exp. Biol.* **215**(4), 657–662 (2012).
30. D. G. Stavenga, “The wing scales of the mother-of-pearl butterfly, *Protogoniomorpha parhassus*, are thin film reflectors causing strong iridescence and polarization,” *J. Exp. Biol.* **224**(15), jeb242983 (2021).
31. D. G. Stavenga, “Thin film and multilayer optics cause structural colors of many insects and birds,” *Mater. Today: Proc.* **1**, 109–121 (2014).
32. C. Kilchoer, U. Steiner, and B. D. Wilts, “Thin-film structural coloration from simple fused scales in moths,” *Interface Focus* **9**(1), 20180044 (2019).
33. G. Guidetti, H. Sun, B. Marelli, *et al.*, “Photonic paper: multiscale assembly of reflective cellulose sheets in *Lunaria annua*,” *Sci. Adv.* **6**(27), eaba8966 (2020).
34. C. J. van der Kooi, J. T. M. Elzenga, J. Dijksterhuis, *et al.*, “Functional optics of glossy buttercup flowers,” *J. R. Soc. Interface* **14**(127), 20160933 (2017).
35. I. Casser, B. Steffan, and W. Steglich, “The chemistry of the plasmodial pigments of the slime mold *Fuligo septica* (Myxomycetes),” *Angew. Chem. Int. Ed. Engl.* **26**(6), 586–587 (1987).
36. B. Steffan, M. Praemassing, and W. Steglich, “Physarochrome A, a plasmodial pigment from the slime mould *Physarum polycephalum* (myxomycetes),” *Tetrahedron Lett.* **28**(32), 3667–3670 (1987).

37. M. Stoyneva-Gärtner, B. Uzunov, M. Androv, *et al.*, “Potential of slime molds as a novel source for the cosmetics industry,” *Cosmetics* **10**(1), 3 (2022).
38. B. Czczuga, “Investigations on carotenoids in fungi VII. Representatives of the myxomycetes genus,” *Nova Hedwigia* **32** (1980).
39. P. Loganathan, P. Paramasivan, and I. Kalyanasundaram, “Melanin as the spore wall pigment of some myxomycetes,” *Mycol. Res.* **92**(3), 286–292 (1989).
40. M. Poulain, M. Meyer, and J. Bozonnet, “Les myxomycètes, vol. 1–2,” Sevrier: Fédération mycologique et botanique Dauphiné-Savoie (2011).
41. A.-M. Fiore-Donno, C. Berney, J. Pawlowski, *et al.*, “Higher-order phylogeny of plasmodial slime molds (Myxogastria) based on elongation factor 1-A and small subunit rRNA gene sequences,” *J. Eukaryotic Microbiol.* **52**(3), 201–210 (2005).
42. A. M. Fiore-Donno, A. K. Tice, and M. W. Brown, “A non-flagellated member of the Myxogastria and expansion of the Echinosteliida,” *J. Eukaryotic Microbiol.* **66**(4), 538–544 (2019).
43. S. Kinoshita, S. Yoshioka, and J. Miyazaki, “Physics of structural colors,” *Rep. Prog. Phys.* **71**(7), 076401 (2008).
44. T. Sai, M. Saba, E. R. Dufresne, *et al.*, “Designing refractive index fluids using the Kramers–Kronig relations,” *Faraday Discuss.* **223**, 136–144 (2020).
45. B. D. Wilts, B. Wijnen, H. L. Leertouwer, *et al.*, “Extreme refractive index wing scale beads containing dense pterin pigments cause the bright colors of pierid butterflies,” *Adv. Opt. Mater.* **5**(3), 1600879 (2017).
46. G. W. Martin, “The myxomycetes,” *Bot. Rev.* **6**(7), 356–388 (1940).
47. F. Schuster, “Electron microscope observations on spore formation in the true slime mold *Didymium nigripes*,” *J. Protozool.* **11**(2), 207–216 (1964).
48. J. J. McCormick, J. C. Blomquist, and H. P. Rusch, “Isolation and characterization of a galactosamine wall from spores and spherules of *Physarum polycephalum*,” *J. Bacteriol.* **104**(3), 1119–1125 (1970).
49. V. V. Vogler-Neuling, M. Saba, I. Gunkel, *et al.*, “Biopolymer photonics: From nature to nanotechnology,” *Adv. Func. Mater.* 2306528 (2023).
50. J. D. Schoknecht and H. W. Keller, “Peridial calcification in the Myxomycetes,” in *Origin, Evolution, and Modern Aspects of Biomineralization in Plants and Animals*, (Springer, 1989), pp. 455–488.
51. J. D. Schoknecht, “SEM and X-ray microanalysis of calcareous deposits in myxomycete fructifications,” *Transactions of the American Microscopical Society* pp. 216–223 (1975).
52. R. K. Nelson, R. W. Sheetz, and C. J. Alexopoulos, “Elemental composition of *Metatrachia vesparium* sporangia,” *Mycotaxon* **5**, 365–376 (1977).
53. C. Chen, C. A. Airolidi, C. A. Lugo, *et al.*, “Flower inspiration: Broad-angle structural color through tunable hierarchical wrinkles in thin film multilayers,” *Adv. Funct. Mater.* **31**(5), 2006256 (2021).
54. P. Freyer, B. D. Wilts, and D. G. Stavenga, “Cortex thickness is key for the colors of iridescent starling feather barbules with a single, organized melanosome layer,” *Front. Ecol. Evol.* **9**, 746254 (2021).
55. A. Donges, “The coherence length of black-body radiation,” *Eur. J. Phys.* **19**(3), 245–249 (1998).
56. C. Rojas and S. L. Stephenson, *Myxomycetes: biology, systematics, biogeography and ecology* (Academic Press, 2021).
57. A. Ronikier, P. Janik, M. de Haan, *et al.*, “Importance of type specimen study for understanding genus boundaries—taxonomic clarifications in *Lepidoderma* based on integrative taxonomy approach leading to resurrection of the old genus *Polyschismium*,” *Mycologia* **114**(6), 1008–1031 (2022).
58. I. García-Cunchillos, B. Estébanez, and C. Lado, “Spore ultrastructural features and significance of their diverse ornamental elements in the evolutionary history of the order Trichiales (Myxomycetes, Amoebozoa),” *Eur. J. Protistol.* **81**, 125839 (2021).
59. P. Janik and A. Ronikier, “Meriderma species (Myxomycetes) from the Polish Carpathians: a taxonomic revision using SEM-visualized spore ornamentation,” *Acta Soc. Bot. Poloniae* **85**(1), 1 (2016).
60. G. Jacucci, S. Vignolini, and L. Schertel, “The limitations of extending nature’s color palette in correlated, disordered systems,” *Proc. Natl. Acad. Sci.* **117**(38), 23345–23349 (2020).
61. S. Mann and G. A. Ozin, “Synthesis of inorganic materials with complex form,” *Nature* **382**(6589), 313–318 (1996).
62. S. Mann, *Biomineralization: principles and concepts in bioinorganic materials chemistry* (Oxford University Press, 2001).
63. L. Kabalah-Amitai, B. Mayzel, Y. Kauffmann, *et al.*, “Vaterite crystals contain two interspersed crystal structures,” *Science* **340**(6131), 454–457 (2013).
64. L. Li, S. Kolle, J. C. Weaver, *et al.*, “A highly conspicuous mineralized composite photonic architecture in the translucent shell of the blue-rayed limpet,” *Nat. Commun.* **6**(1), 6322 (2015).
65. N. Nassif, N. Pinna, N. Gehrke, *et al.*, “Amorphous layer around aragonite platelets in nacre,” *Proc. Natl. Acad. Sci.* **102**(36), 12653–12655 (2005).
66. H.-B. Yao, J. Ge, L.-B. Mao, *et al.*, “25th anniversary article: artificial carbonate nanocrystals and layered structural nanocomposites inspired by nacre: synthesis, fabrication and applications,” *Adv. Mater.* **26**(1), 163–188 (2014).
67. R. Quintero-Torres, J. Aragón, M. Torres, *et al.*, “Strong far-field coherent scattering of ultraviolet radiation by holococcolithophores,” *Phys. Rev. E* **74**(3), 032901 (2006).
68. P. Vukusic and J. R. Sambles, “Photonic structures in biology,” *Nature* **424**(6950), 852–855 (2003).

69. X. Li, J. Peoples, Z. Huang, *et al.*, "Full daytime sub-ambient radiative cooling in commercial-like paints with high figure of merit," *Cell Reports Phys. Sci.* **1**(10), 100221 (2020).
70. R. E. Noskov, A. Machnev, I. I. Shishkin, *et al.*, "Golden vaterite as a mesoscopic metamaterial for biophotonic applications," *Adv. Mater.* **33**(25), 2008484 (2021).
71. K. Kitagawa, "Thin-film thickness profile measurement by three-wavelength interference color analysis," *Appl. Opt.* **52**(10), 1998–2007 (2013).
72. A. Ghassaei, "SoapFlow," 1.0, Github, (2021). Accessed: 2023-10-02. <https://github.com/amandaghassaei/SoapFlow/tree/main/python>
73. R. J. Tilley, *Colour and the Optical Properties of Materials* (John Wiley & Sons, 2020).
74. S. Vignolini, E. Moyroud, B. J. Glover, *et al.*, "Analysing photonic structures in plants," *J. R. Soc. Interface* **10**(87), 20130394 (2013).
75. A. Kamono, H. Kojima, J. Matsumoto, *et al.*, "Airborne myxomycete spores: detection using molecular techniques," *Naturwissenschaften* **96**(1), 147–151 (2009).
76. C. J. van der Kooi, A. G. Dyer, P. G. Kevan, *et al.*, "Functional significance of the optical properties of flowers for visual signalling," *Ann. Bot.* **123**(2), 263–276 (2019).
77. C. Lado and U. Eliasson, "Taxonomy and systematics: current knowledge and approaches on the taxonomic treatment of Myxomycetes: updated version," *Myxomycetes* pp. 269–324 (2022).
78. I. García-Cunchillos, J. C. Zamora, M. Ryberg, *et al.*, "Phylogeny and evolution of morphological structures in a highly diverse lineage of fruiting-body-forming amoebae, order Trichiales (Myxomycetes, Amoebozoa)," *Mol. Phylogenetics Evol.* **177**, 107609 (2022).
79. J. García-Martin, J. Zamora, and C. Lado, "Multigene phylogeny of the order Physarales (Myxomycetes, Amoebozoa): Shedding light on the dark-spored clade, in *Persoonia-Molecular Phylogeny and Evolution of Fungi* (Naturalis Biodiversity Center 2023).
80. T. L. Roush, "Estimation of visible, near-, and mid-infrared complex refractive indices of calcite, dolomite, and magnesite," *Icarus* **354**, 114056 (2021).
81. V. Bauernfeind, A. Ronikier, M. Ronikier, *et al.*, "Thin film structural color is widespread in slime molds (Myxomycetes, Amoebozoa) [Data set].," University of Fribourg, 1.0, Zenodo (2024) <https://doi.org/10.5281/zenodo.10000371>.